13

Chemical and Physical Properties of Fluxes for SAW of Low-Carbon Steels

Ana Ma. Paniagua-Mercado and Victor M. Lopez-Hirata
Instituto Politécnico Nacional (ESFM-ESIQIE)
Mexico

1. Introduction

The submerged-arc welding of steels has been used since 1930. It is well known that the mechanical properties of steel weldments depend on the chemical compositions of electrodes and fluxes. The development of welding electrodes has been based on practical experiences. The study of welding deposits by means of physical metallurgy permitted to develop electrodes and fluxes for SAW process of steels. In contrast, the use of chemical and physical properties of fluxes for the development of welding process started in the 70´s. (Shah, 1986). Most of the works concerning with the fluxes for SAW process have been focused on its effect on microstructure and mechanical properties. Likewise, it has been interesting the study of the thermochemical and electrochemical reactions that occur at the welding pool which are very important for the transferring of metallic elements to the welds. In addition to the stated above, the electrode coverings is also a very important aspect to obtain weld metal with good mechanical properties. The covering materials are fluxes which are composed of different mineral chemical compounds such as, oxides, fluorides and carbonates (Singer & Singer, 1979). The firing and sintering process of fluxes during welding electrode processing promotes chemical reactions and phase transformations of these minerals. All these factors determine the valence or electric charge of the different elements which are deposited to the weld metal. All the oxides from flux may contribute to the dissolution process of different metallic elements and oxygen in the welding pool. These metallic elements can react with oxygen to form oxide inclusions which can serve as nucleation sites for the formation of some benefit phases such as acicular ferrite during the welding process (Davis & Bailey 1991). These events may improve the mechanical strength and ductility of weld metal. Thus, the purpose of this chapter is to show the effect of different fluxes on the chemical composition, microstructure and mechanical properties of weld metals by the submerged-arc welding procedure.

2. Chemical and structural characterization of the crystalline phases in agglomerated fluxes for SAW

The weld metal chemistry is affected by the electrochemical reaction at the weld pool flux interface. The main characteristics of submerged-arc welds are a function of the fluxes and their physicochemical properties (Indacochea et al., 1989). Submerged-arc welding (SAW) fluxes are manufactured in three main forms; fused at temperatures exceeding 1400 ºC,

agglomerated from 400 to 900 º C and sintered from 1000 to 1100 º C from mineral constituents, (Jackson, 1982). Reactions, which occur during firing of a ceramic oxide, comprise phase transformations of minerals (Singer, 1963), reaction among the different phases (Allen, 1966), formation of crystal phases from the melt and formation of a melt. The phase transformation of the crystal phases predominates at the early stages of firing, before a melt is formed. The formation of a melt can be observed at temperatures as low as 920 ºC, due to the presence of minor amounts of impurities such as, alkaline earth oxides (Dunham & Christian, 1984). In this way, the agglomerated fluxes can be studied by the chemical analysis of the crystal phases formed during the increase of temperature. This enables us to quantify types of ions and their distribution, which is useful to predict their behavior when they are dissociated in the submerged-arc welding process, (Indacochea et al., 1989). Thus, this section shows a study of the crystalline phases and the chemical characterization of the ions formed in agglomerated fluxes using Chemical Analysis, X-Ray Diffraction (XRD) and Differential Thermal Analysis (DTA). It is also intended to show the effect of ion content of flux on the behavior of submerged-arc welding.

2.1 Composition, preparation and characterization of fluxes

Three agglomerated welding fluxes were prepared, using mixtures of mineral oxides in different proportions (designated as A, B and C), as shown in Table 1. Each mixture was weighed, mixed in a vibratory camera for 30 minutes and subsequently pelletized in a laboratory machine of 80 cm diameter and 28 cm height at 40 rpm, using sodium silicate as the agglomerate agent. The average size of pellets was 5 mm. They were dried in a stove at 200 ºC for 24 hours, fired for 3 hours. at 950 ºC in a gas kiln at a heating rate of 50 ºC/h, crushed and then screened to a 240 μm size. For comparison, a commercial agglomerated welding flux was also used, designated as T sample. The chemical analysis was determined by X-ray fluorescence. The XRD analysis was conducted in a diffractometer with a monochromated Cu Kα radiation. For all the samples, the DTA analysis was carried out in a Al_2O_3 crucible from 25 to 1350ºC at a heating rate of 10ºC/min. Alumina was used as standard reference for DTA analysis.

2.2 Chemical, structural and thermal characterization of fluxes

2.2.1 Chemical analysis

Table 2 shows the elemental chemical composition of the mixtures A, B and C, calculated with the data shown in Table 1 and the stequiometric formula of each compound. Tables 3 and 4 show the elemental chemical analysis and oxide compounds, respectively, for the fused fluxes A, B, C and T. By comparison of Table 1 with Table 3, it can be noticed that there was an increase in the percentage of Al_2O_3, SiO_2, and Na_2O. These oxides increased at the same proportion as they were present in the original mixtures. This can be attributed to the evaporation of impurities such as alkaline oxides with a low melting point that were present in the original mineral, (Dunham & Christian, 1984). The amount of CaO showed the highest decrease because it came from the $CaCO_3$ compound, in the original mixture, which is decomposed at about 900 °C (Singer, 1963). The Na_2O also is formed from Na_2CO_3, but its proportion is a little higher than the original one because the sodium silicate, Na_2SiO_4, was used for the agglomerating process. In order to be agglomerated, a higher amount of sodium silicate was added to the flux B than that added to the fluxes A and C. This fact explains the difference in Na_2O composition.

In the SAW process, the temperature of electric arc causes the dissociation of oxides and these remains as ions in the plasma, (Belton et al. 1963). The temperature in the welding pool reaches 1560-2300 °C. Christensen and Gjermundsen, (Christensen & Gjermundsen, 1962) calculated temperatures above 2500 °C for the welding pool in mild steels. Apold (Apold, 1962) suggested that the heat energy provided by the electric arc is concentrated on a circumference of 5mm diameter. According to the above information, most of the oxides are melted, but oxides with high melting points such as MgO (2500-2800 °C), CaO (2572 °C) and ZrO_2 (2720 °C) are not melted. That is, it is important that the chemical formulation of fluxes enables all the oxides to be melted in order to avoid the presence of inclusion in the weldment.

Compounds	Flux A	Flux B	Flux C
Al_2O_3	2.6	8.00	8.0
SiO_2	43.8	25.00	20.0
Fe_2O_3	6.0	2.0	9.0
K_2O	0.11	0.07	0.07
Na_2CO_3	0.09	1.0	0.20
$CaCO_3$	20.00	3.0	5.0
MnO	7.00	---	11.0
MgO	6.00	1.0	5.0
TiO_2	10.00	29.00	31.00

Table 1. Initial composition (wt. %) of fluxes.

Element	Flux A	Flux B	Flux C	Flux T
Al	3.85	12.17	12.00	9.71
Si	25.53	14.72	11.47	5.46
Fe	1.74	0.52	2.74	2.4
K	0.37	0.24	0.24	0.32
Na	1.05	10.4	2.36	0.9
Ca	8.1	1.21	1.88	4.85
Mn	4.11	-	6.38	9.2
Mg	2.8	0.37	2.49	4.47
C	0.46	0.53	0.03	0.08
S	0.08	0.028	0.06	0.016
Ti	5.3	15.5	16.7	21.6

Table 2. Elemental chemical analysis (wt. %) of fused fluxes.

Oxide	Flux A	Flux B	Flux C	Flux T
Al_2O_3	7.29	23.00	23.00	18.36
SiO_2	54.65	31.50	24.50	11.69
Fe_2O_3	2.48	0.74	3.92	3.43
K_2O	0.44	0.28	0.28	0.38
Na_2O	1.41	14.00	3.18	1.21
CaO	11.33	1.69	2.63	6.78
MnO	5.30	-	8.23	11.88
MgO	4.64	0.61	4.12	7.41
TiO_2	9.00	26.00	28.00	36.31

Table 3. Oxide compound (wt. %) of fused fluxes.

2.2.2 Structural analysis

Figures 1, 2, 3 and 4 shows the X-ray diffraction patterns of agglomerated and sintered fluxes. Here, it can be observed the presence of crystalline phases, such as Nepheline ($NaAlSiO_4$), Gismodine ($CaAl_2Si_2O_8.4H_20$) and Vesuvianite ($Ca_{19}AI_{II}Mg_2Si_{18}O_{69}(OH)_9$), which were formed at low temperature, (Berry & Mason, 1959). These are equilibrium phases and were formed due to the reaction at the sintered temperature between different ions of the original mixture with the sodium silicate, added during the agglomeration process. Other oxides, such as titanium oxide and manganese oxide showed practically no reaction with other reactants at these temperatures; however, they appeared with a different oxidation degree and crystalline structure. The silicon oxide, aluminum oxide and calcium oxide did not react at all.

The Nepheline phase can be formed by replacement of the half of silicon atoms with aluminum atoms in the sodium silicate compound, (Klein & Hurbult, 1999). The electric balance is kept by the addition of sodium ions in the interstitial sites of the hexagonal structure (Berry & Mason, 1959). Its quantification is shown in Table 4 and it was based on the X-ray diffraction peaks with the highest intensity (Cullity, 2003). Table 5 shows the quantification of ions calculated according to its disassociation reaction at the temperature of electric arc, as proposed by Davis and Bailey (Davis & Bailey, 1991).

The Gismodine phase can be melted at low temperatures and has a monoclinic structure and also appeared in the sintered fluxes. The quantification of compound and ions is shown in Tables 4 and 5, respectively.

The Vesuvianite phase has a low melting point and tetragonal crystalline structure. This could be formed by means of the replacement of aluminium with silicon. This phase has also a low melting temperature and a tetragonal structure. Its quantification is also shown in Tables 4 and 5.

The other detected phases were Quartz, Rutile, Anastase and γ-titanium oxide. Fluorite was only detected in the flux T. All these compounds showed practically no reaction at the sintering temperature. These were also stable at room temperature. Tables 4 and 5 show their quantification as ions and compounds, respectively.

The formation of different oxides and silicates observed in fluxes A, B and C, but not in flux T can be attributed to the addition of sodium silicate used in the agglomeration process of the former fluxes, as well as the high sintering temperature.

2.2.3 Thermal analysis

All oxides were stable during heating of DTA up to 1000 °C. Thus, the DTA curves are shown in the range of 1000-1350°c for fluxes A, B, C and T in Figs. 5, 6, 7 and 8, respectively. Most of the reactions observed in DTA curves were endothermic type. Some of the endothermic peaks are located at close temperature values for the different fluxes. For instance, an endothermic peak is located at 1147.8, 1121.4, 1122.3 and 1161.6 °C for the fluxes A, B, C and T, respectively. Another one is located at 1226.0, 1189.3, 1213.4 and 1228.6 °C for the same fluxes, respectively. Finally, a peak located at 1288.4, 1267.9 and 1286.6 °C for the fluxes B, C and T, respectively. The difference in temperature for these endothermic events can be attributed to the difference in chemical composition of fluxes.

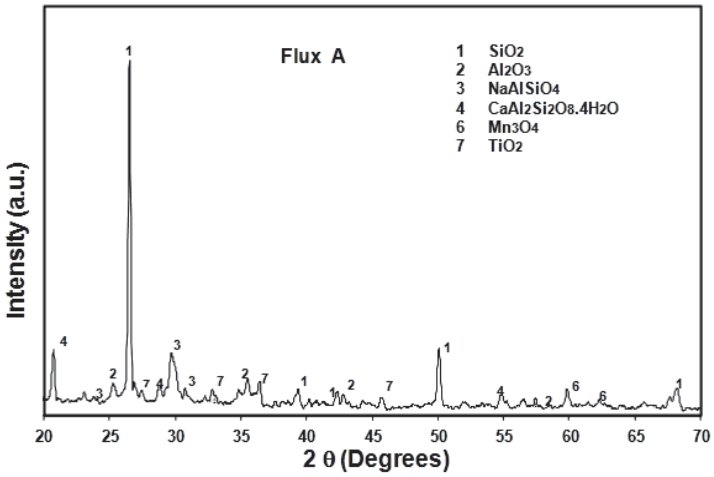

Fig. 1. XRD pattern of the flux A.

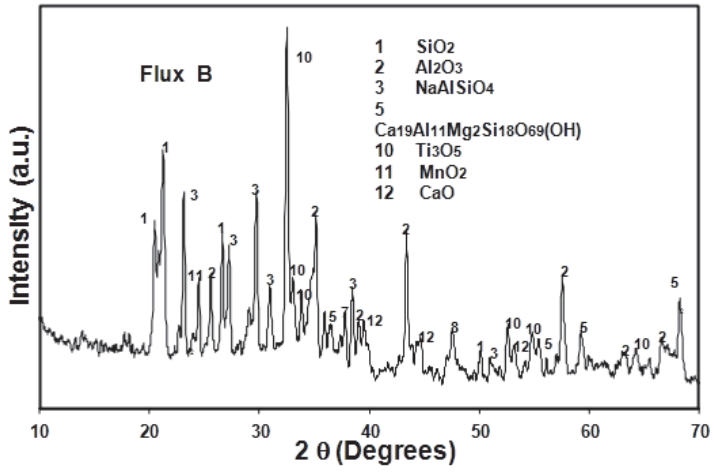

Fig. 2. XRD pattern of the flux B.

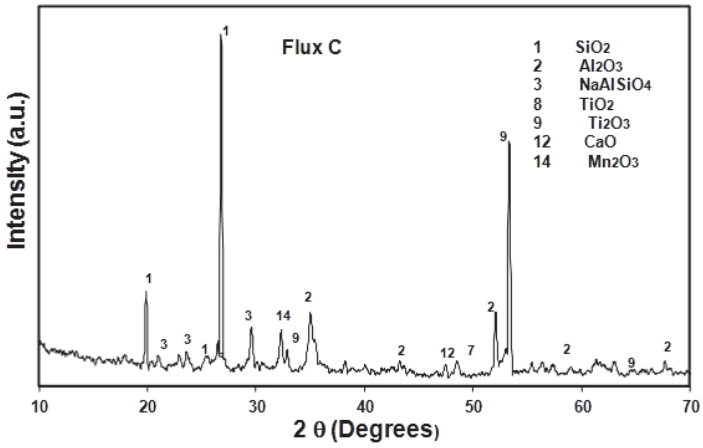

Fig. 3. XRD pattern of the flux C.

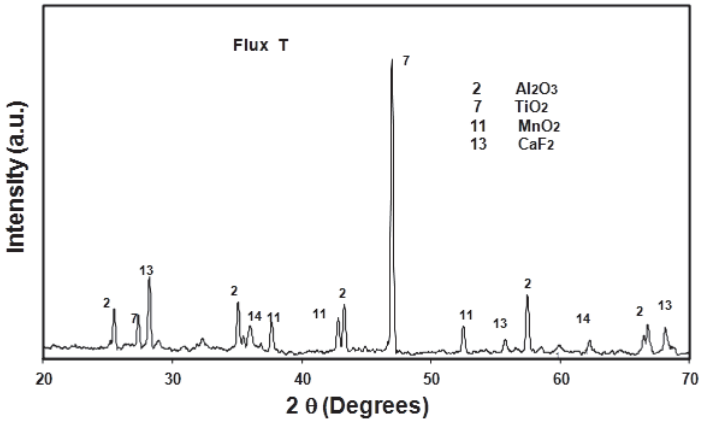

Fig. 4. XRD pattern of the flux T.

Name	Composition	A	B	C	T
Corundum	Al_2O_3	9.17	17.90	12.11	19.07
Quartz	SiO_2	51.10	17.05	18.38	6.90
Nepheline	$NaAlSiO_4$	12.65	19.95	17.12	-----
Gismondine	$CaAl_2Si_2O_8.4H_20$	12.65	-----	-----	-----
Vesuvianite	$Ca_{19}AI_{11}Mg_2Si_{18}O_{69}(OH)_9$	-----	10.23	-----	-----
Hausmannite	Mn_30_4 $[MnOMn_2O_3]$	5.24	3.80		6.10
Anatase	TiO_2	-----	6.95	3.60	53.03
Rutile	TiO_2	9.17	-----	-----	-------
γ-Titanium oxide	$Ti_3\ 0_5$	-----	20.32	-----	-------
Titanium oxide	Ti_20_3	-----	-----	25.65	--------
Manganese oxide	Mn_2O_3	----	-----	8.55	-------
Calcium oxide	CaO			3.56	
Fluorite	Ca F_2	-----	-----	----	14.90

Table 4. Weight percent of compounds determined from XRD.

Ion	Flux A	Flux B	Flux C	**Flux T**
% Al^{+3}	10.51	14.28	11.01	10.09
% Si^{+4}	29.55	22.80	19.79	3.22
% Na^{+}	2.05	3.23	1.15	---
% Mn^{+2}	1.17	0.84	2.65	1.36
% Mn^{+3}	2.60	1.88	5.90	3.03
% Mn^{+4}				
% Ti^{+2}	5.5	6.95	2.15	31.79
% Ti^{+3}			17.08	
% $Ti^{5/3}$		13.05		
% Ca^{+2}	2.34	2.57	2.54	7.64
% Mg^{+2}		1.88		
% H^{+1}	0.12	0.03		
% F^{-1}				7.26
% O^{-2}	46.16	42.21	32.47	35.61

Table 5. Ion content (mol %) of fluxes.

The endothermic reactions corresponding to the above temperatures can be compared with the melting reaction of Gismodine, which has been reported to occur in a temperature range between 965 and 1082 °C. Quartz transformation from Cristobalite to Tridimite occurs between 1200 and 1650 °C. Na_2O sublimation takes place at about 1275 °C. Fluorite and

Vesuvianite melt at about 1200 °C. Nefeline melts at temperatures higher than 1248 °C. The melting of corundum, rutile, anastase, hausmannite and quartz was not detected because it occur above 1500 °C. The zigzag behavior of DTA curves reveals blistering or gassing of the glass formation (Gordon & Chu, 1966).

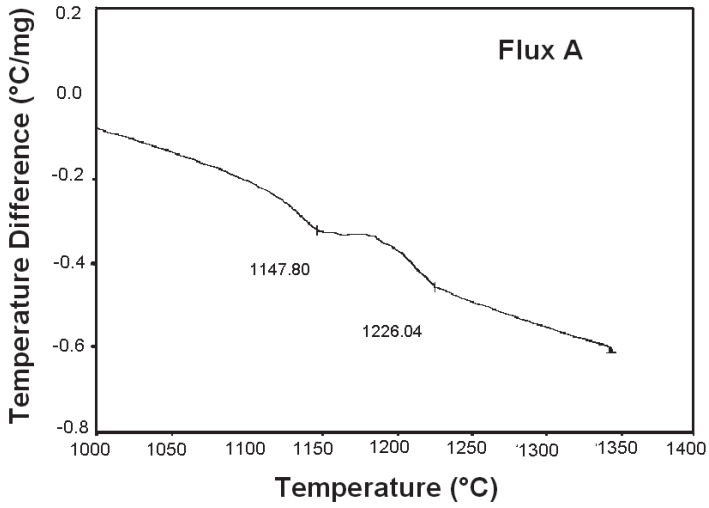

Fig. 5. DTA diagram of flux A.

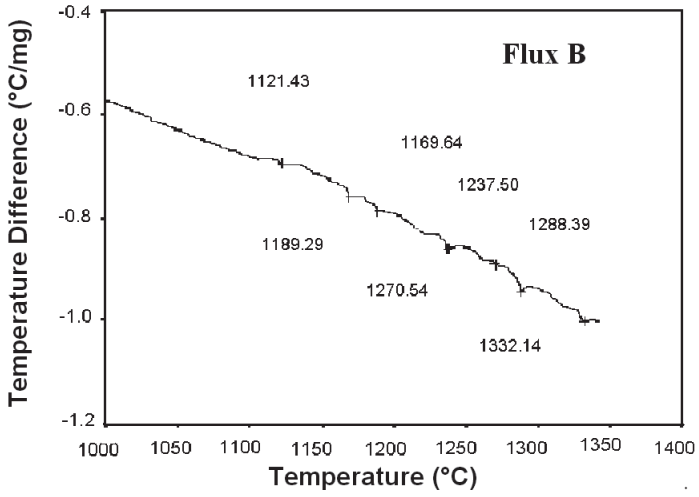

Fig. 6. DTA diagram of flux B.

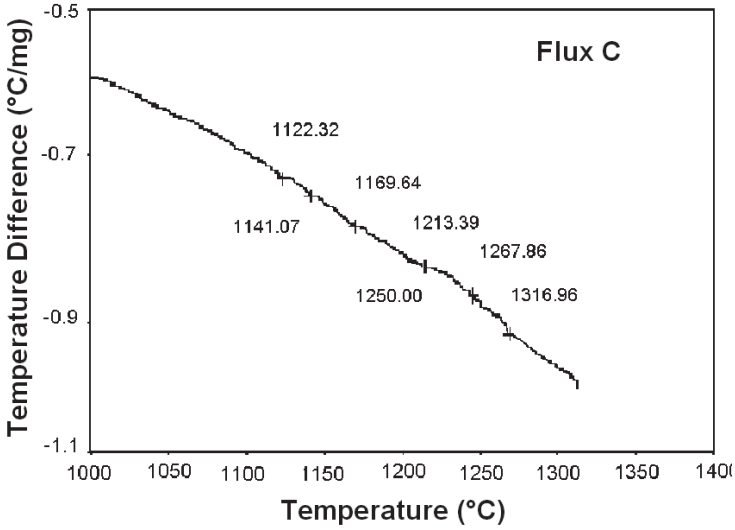

Fig. 7. DTA diagram of flux C.

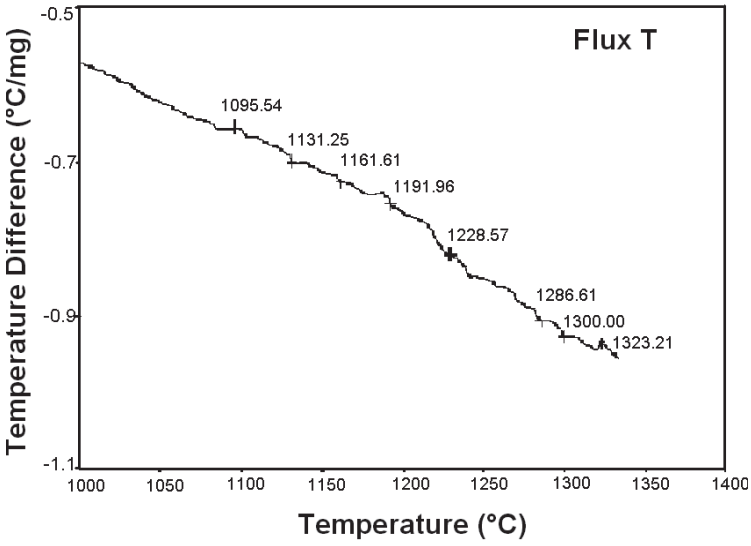

Fig. 8. DTA diagram of flux T.

2.3 Effect of crystalline phases and ion contents on the behavior of flux

Oxides and carbonates were used for manufacturing the different fluxes. These formed different crystalline phases after sintering. According to the X-ray diffraction analyses, silica (SiO_2), manganese oxide (MnO) and titanium oxide (TiO_2) were the compounds that reacted during the heating of fluxes.

The silica reacted to form anionic species such as silicates. Three compounds with this characteristic were identified in the sintered fluxes: Nepheline ($NaAlSiO_4$), Gismodine ($CaAl_2Si_2O_8.4H_2O$) and Vesuvianite ($Ca_{19}Al_{11}Mg_2Si_{18}O_{69}.(OH)_9$). The silicon electrodeposition in the welding cathodic pool is not as favored as the deposition of volatile calcium from flux. It has been found (Davis & Bailey, 1991) that a small amount of silicon can be formed electrochemically, but most of it is formed by means of calcium evaporation, which can reduce the SiO_2 in the flux.

It was found that the hausmannite (Mn_3O_4) was formed in the sintered fluxes. This is a spinel with electron valences, Mn^{+2} and Mn^{+3}. Thus, it is possible to have different reactions which permit the formation of several oxide compounds and oxide radicals from MnO, forming inclusions.

The ion quantification determined from the X-ray diffraction results enables us to estimate the amount of the ions from flux formed in the plasma of electric arc. These ions react with oxygen and the oxides will be deposited on the weld. The most important reactions between the electric arc and welding pool correspond to those where oxygen is involved.

Oxygen can react with any cationic component from the flux, as Na^{+1}, Ca^{+2}, Mg^{+2}, Al^{+3}, Si^{+4}, Fe^{+2}, Fe^{+3}, Mn^{+2}, Mn^{+3}, Mn^{+4}, Ti^{+2}, Ti^{+3}, $Ti^{+5/3}$ and probably SiO_4^{-4} from the silicates formed in the fluxes, the anions present are O^{-2} and F^{-1}.

It is possible to make a prediction of the reactions with these cations and anions. Calcium and magnesium are expected to react first with oxygen in the welding arc because its corresponding oxides have the largest negative formation free energy ΔG_f. Al^{+3} has the next highest value for the formation of a stable oxide. Si^{+4} and Titanium reacts readily with oxygen in the next order. Ti^{+2} almost react at the same time with Mg^{+2}, and then Ti^{+3} and Ti^{+4} react to form stable dioxides to give anions and cations with similar set of reactions. Manganese too exhibit variable valency and may form many oxides and oxide radicals when react with the oxygen in the next order Mn^{+2}, Mn^{+3} and Mn^{+4} in agreement with the corresponding ΔG_f values (Davis & Bailey, 1991).

The silicates formed will be more soluble in the slag than in the weld pool. Transfer of Mn, Si and Al from the flux to weld pool depends on the amounts in the flux (Davis & Bailey, 1991).

The oxygen can react with any available cationic species to give non-metallic inclusions.

The identification of phases in fluxes can be used to know the behavior of fluxes during their depositing process, as well as the effect of them on the mechanical properties of welds.

In the fluxes A, B, C, and T, the presence of corundum can be observed, which has an effect on the facility for slag removing (Jackson, 1982). The same effect has been observed for the presence of rutile in fluxes.

Calcium ions in fluxes increase the stability of electric arc (Butler & Jackson, 1967). These ions can come from either oxide or fluoride compounds. Significant calcium content was detected for fluxes A, C and T but not for flux B. Thus, the latter might present an unstable electric arc during welding.

It is also known that quartz and corundum increase the viscosity of fluxes, while the additions of manganese oxide, fluorite and titanium oxide reduce viscosity (Jackson, 1982).

The latter compounds were detected in the fluxes A, C, and T, but only a small content, may be as impurity, and were observed in the flux B. Thus, a problem of flux fluidity might be present in this flux.
The manganese oxide and quartz have been observed to have a beneficial effect on the mechanical properties of welds (Lancaster, 1999). Manganese oxide and quartz were included in the formulation of fluxes A and C, but not for flux B.
Titanium oxide has been observed to promote the formation of acicular ferrite, which is less susceptible to cracking (Evans, (1996). Fluxes C and T are expected to produce the better weld since they contain quartz, manganese oxide, titanium oxide, and the content of oxygen ions (calculated by X-ray diffraction) is smaller than A and B.

2.4 Influence of chemical composition on the microstructure and tensile properties of SAW welds

The mechanical properties of welds are determined by the microstructure developed during the submerged-arc welding process (Joarder et al. 1991). It was suggested that the acicular ferrite provided a good toughness and tensile strength to the welds because its fine size has a higher resistance to the crack propagation (Liu & Olson, 1986). Thus, it seems to be convenient to increase the volume fraction of ferrite in welds. Widmanstätten, equiaxial and acicular ferrite can be developed by the welding process. A method for promoting the formation of acicular ferrite consists of the additions of oxides into the flux, such as boron oxide, vanadium oxide and titanium oxide (Evans, 1996). The oxides in the flux may contribute to different metallic element dissolution and oxygen into the weld. These elements may react to form oxide inclusions, which are trapped into the weld and facilitate the nucleation of acicular ferrite during the weld cooling (Dowling et al. 1986) and (Vander et al. 1999). The main factors that determine the microstructure of a weld are: chemical composition, austenite grain size and cooling rate (Lancaster, 1980). The chemical composition comes from the composition of base metal, electrode and flux (Davis & Bailey, (1991). In order to increase the mechanical properties of welds for low-carbon steels, the selection of an appropriate flux composition plays a very important role to obtain a fine acicular ferrite, which has been shown to improve the properties in this type of welds. The objective of this work is to study the effect of different fluxes on the chemical composition, microstructure and tensile properties of weld applied on an AISI 1025 steel by the arc-submerged welding process.

2.4.1 Weldment preparation and mechanical tests

The chemical composition of fluxes used in this work are given in Table 6. It also includes the composition for a commercial flux to be used for comparison purposes. The compositions were selected in order to analyze the effects of SiO_2, MnO and TiO_2 on weld properties. The base metal was a 250 x 60 x 13 mm plate of an AISI 1025 steel, with a chemical composition as given in Table 7. The joint preparation was a 45° single V-groove. The welding fluxes were dried at 200 °C for 24 hours. The welding conditions were 600 A, 30V and a welding speed of 0.118 ms^{-1}, and kept constant for all cases. All welds were carried out in one pass. Tension specimens were extracted from welded plates and prepared according to the E8M-86 ASTM standard. Tension tests were conducted at room temperature and 3.33×10^{-4} s^{-1} in a universal machine and on 10 specimens for each flux. Vickers hardness measurements were carried out on the base metal, heat affected zone and weld site with a load of 10 kg. The chemical analysis of welds was performed by an X-ray

fluorescence spectrometer. Weld samples were prepared metallographically and etched with Nital to be observed in a Scanning Electron Microscope (SEM) at 20 kV and a light microscope. Microanalysis were also carried out on the inclusions of welds using an EDX equipment attached to the SEM. Macroetching was also carried out with Nital reagent.

Flux	wt.% SiO_2	wt.% Fe_20_3	wt.% MnO	wt.% MgO	wt.% K_2O	wt.% Na_2O	wt.% CaO	wt.% Al_2O_3	wt.% TiO_2
A	54.65	2.48	5.30	4.64	0.44	1.41	11.33	7.29	9.00
B	31.51	0.74	---	0.61	0.28	14.00	1.69	23.00	26.00
C	24.55	3.92	8.23	4.12	0.28	3.18	2.63	23.0	28.0
T	11.69	3.43	11.88	7.41	0.38	1.21	6.78	18.36	36.31

Table 6. Chemical composition of fluxes.

2.4.2 Chemical composition

As is well known, the reactions between liquid weld metal and fused flux in the SAW process are similar to those between molten metal and slag in the steel making process. As shown in Table 7, the manganese, silicon, calcium, titanium and aluminum contents of the weld metal increase as the content of the corresponding oxides for the initial flux also increases. It was reported (ASM, *Metals Handbook*, 1989) that a rapid pick up of manganese and silicon might occur until its corresponding oxide content of the flux was about, 10 and 40 %, respectively. The fluxes T and A have the highest contents of MnO and SiO2, respectively. The highest contents of manganese and silicon were also detected for the weld metal of fluxes T and A, respectively.

The lowest carbon content was detected for the weld metals of the fluxes B and C. This is attributed to the higher contents of Al_2O_3 and SiO2 for those fluxes, which give a higher content of O^{-2} ions that react with carbon (Davis & Bailey, 1991). Additionally, these fluxes also have the lowest content of metallic cations.

2.4.3 Mechanical properties

Table 8 shows the average values of tensile properties, yield strength (S_y), ultimate tensile strength (S_{uts}), elongation percentage and area reduction percentage. The Vickers hardness at the center of weld is also shown in this table.

The tensile strength and hardness of a steel can be related to the equivalent carbon, given by the following equation (Zhang et al. 1999):

$$C_{equivalent} = C + Mn/6 + Si/24 + Ni/40 + Cr/5 + Mo/4 + V/4 \quad (1)$$

Where C, Mn, Si, Ni, Mo and V represent the metallic content, expressed as a percentage. As expected, the highest and lowest tensile strength and hardness were obtained for the weld metal with the highest and lowest equivalent carbon, respectively. It was reported, (Lancaster, 1980) that an equivalent carbon higher than 0.45 had a high susceptibility to cold cracking after welding. Besides, the formation of martensite is facilitated during cooling of welds. The equivalent carbon of welds for all fluxes is lower than 0.45. The highest toughness, detected by the largest area under the engineering stress-strain curve, corresponded to the weld metals of fluxes T and C. This can be attributed to their higher content of manganese, which is known to improve the steel toughness (ASM, *Metals Handbook*, 1989). Table 8 also shows the yield and ultimate tensile strengths calculated using

a computer program based on a non-linear multiparameter regression of the strength versus the composition (Material Algorithms Project, 1999). The calculated values are higher than the values determined in this work. The differences can be attributed to the fact that the regression program considers neither the cooling condition of the weld nor the microstructure constituents. Nevertheless, the highest and lowest calculated yield and ultimate tensile strengths also corresponded to the welds for fluxes T and B, respectively.

Element (wt. %)	Base Metal	Electrode	Weld (Flux A)	Weld (Flux B)	Weld (Flux C)	Weld (Flux T)
C	0.248	0.082	0.124	0.103	0.098	0.171
Mn	0.785	1.312	0.640	0.710	1.000	1.380
Si	0.218	0.762	0.610	0.300	0.470	0.530
P	0.024	----	0.008	0.008	0.10	0.019
S	0.037	0.008	0.0044	0.034	0.046	0.033
Mo	0.016	---	0.006	0.006	0.006	0.012
Ni	0.118	----	0.030	0.030	0.030	0.090
Cu	0.345	----	0.175	0.130	0.134	0.285
Sn	0.048	----	0.004	0.004	0.004	0.022
Al	----	----	0.004	0.027	0.001	0.010
Ti	0.002	----	----	---	0.020	0.023
As	----	----	0.004	0.004	0.006	0.007
Ca	----	----	0.0031	----	0.002	0.0007
Cr	0.0054	----	----	----	----	0.090
V	0.004	----	----	----	----	----

Table 7. Chemical composition of steel, electrode and welds.

Flux	S_y (MPa)	S_{uts} (Mpa)	Elongation (%)	Area Reduction (%)	Vickers Hardness	$C_{equivalent}$	Calc. S_y (MPa)	Calc. S_{uts} (MPa)
A	208	410	22	47	167	0.28	446	572
B	197	418	23	51	163	0.24	407	507
C	330	551	19	36	179	0.30	565	583
T	345	569	20	43	192	0.43	586	662

Table 8. Tensile properties, hardness an equivalent carbon of welds for the different fluxes.

2.4.4 Macrostructure and microstructure of welds

The macrographs of the as-deposited region of welds corresponding to the fluxes A, B, C and T show a dendrite structure. The width of the heat affected zone (HAZ) is about 0.4 mm for most of the welds. In the case of HAZ, the ferrite mean grain size is about 5-9 μm. Figures 9 (a)-(d) and (e)-(h) show the light and SEM micrographs, respectively, of the welds corresponding to the fluxes A, B, C and T. Table 9 summarized the microconstituents and its volume percentage observed in the welds corresponding to the fluxes A, B, C and T. Pearlite and equiaxial ferrite are observed for all welds. No Widmanstätten ferrite is detected for all

welds. The acicular ferrite was only detected for the welds corresponding to the fluxes C and T. This can be attributed to the TiO_2 content of flux because this type of oxides favored the nucleation of acicular ferrite at the interface between austenite matrix and inclusion (Zhang et al. 1999) and (Babu et al. 1999). Table 9 also shows the calculated microstructure constituents using a computer program based on the weld composition and welding conditions (current, voltage and welding speed), (Material Algorithms Project, 1999). According to the calculated results, no Widmanstätten ferrite is predicted to be formed for these weld compositions, which is in agreement with the results described above. However, the calculated results indicated no presence of Pearlite, which can be observed clearly for all welds in Fig. 9. The calculated microstructure results also show the increase in the volume percentage of bainite + acicular ferrite for the fluxes C and T, compared with microstructure results for fluxes A and B. This fact shows a good agreement with the presence of acicular ferrite observed for the welds corresponding to fluxes C and T.

The volume percentage of inclusions is show in Table 10 for the welds corresponding to fluxes A, B, C, and T. The lowest and highest contents of inclusions are detected for the welds of fluxes C and T, and those of fluxes A and B, respectively. Table 10 also shows the content of oxygen ions, calculated from the flux composition. The lower the content of oxygen ions, the lower inclusion content in the weld steel is resulted. The elongation and area reduction percentages are shown to have a dependence on with the inclusion volume percentage. This seems to be reasonable since the ductility is drastically decreased with the increase of inclusions in steels (Liu & Olson, 1986).

Weld	Equiaxial Ferrite (%)	Widmast. Ferrite (%)	Pearlite (%)	Acicular Ferrite (%)	Calculated Widmanst. Ferrite (%)	Calculated Ferrite (%)	Calculated Acic. Ferrite+Bainite (%)
Flux A	83	0	17	0	0	1.85	98.15
Flux B	88	0	12	0	0	1.97	98.03
Flux C	69	0	20	11	0	1.86	98.14
Flux T	68	0	8	24	0	1.24	98.76

Table 9. Microstructure of welds.

Weld	O^{-2} ion %	Basicity Index	Inclusion vol. %
Flux A	46.16	0.35	24.40
Flux B	46.21	0.30	21.60
Flux C	32.47	0.32	15.00
Flux T	35.61	0.60	15.11

Table 10. Content of inclusions.

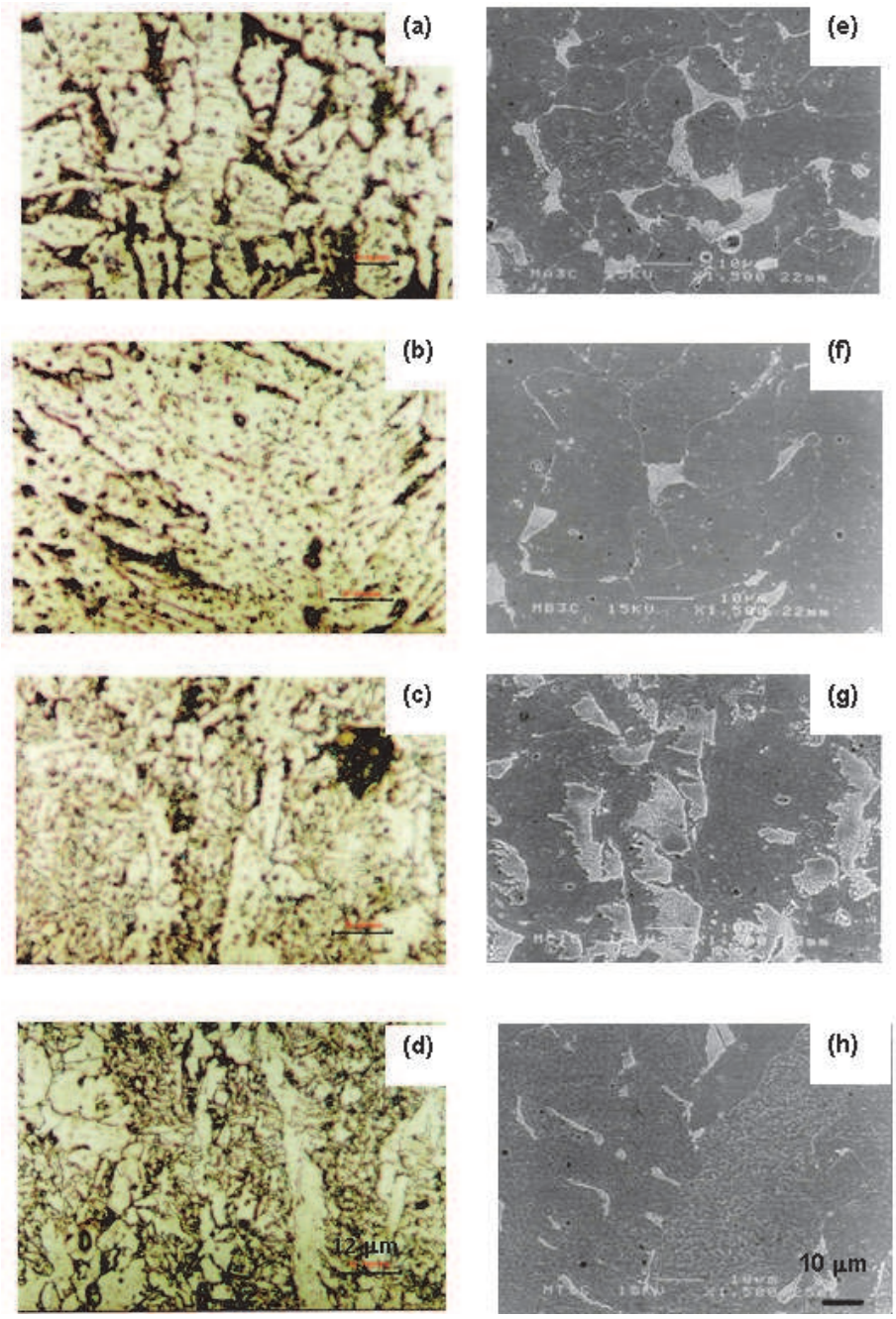

Fig. 9. Light and SEM micrographs of welds for (a) and (e) flux A, (b) and (f) flux B, (c) and (g) flux C, and (d) and (h) flux T, respectively.

The microanalysis on inclusions indicated that most of inclusions are aluminum and silicon oxides, manganese and calcium sulfides; however, the presence of round and bright titanium oxide inclusions is observed only for the welds of fluxes C and T, Fig. 10. This type of inclusions were mainly composed of Ti, Al, Mn and Si. This fact suggests that the acicular ferrite seems to be nucleated at the interface between austenite matrix and titanium oxide inclusions welds. We believe that almost no TiO_2 inclusions are formed for welds of fluxes A and B because these fluxes have the lowest content of MnO. MnO was reported (Davis & Bailey, 1991), to react with SiO_2 to form silicomanganates. However, the absence of MnO causes SiO_2 to react with TiO_2 to form silicotitanates. Thus, this may explain the absence of acicular ferrite for welds corresponding to fluxes A and B. The titanium-containing welds corresponding to fluxes C and T have the highest yield and ultimate tensile strengths. This fact is in agreement with the formation of acicular ferrite observed for these welds.

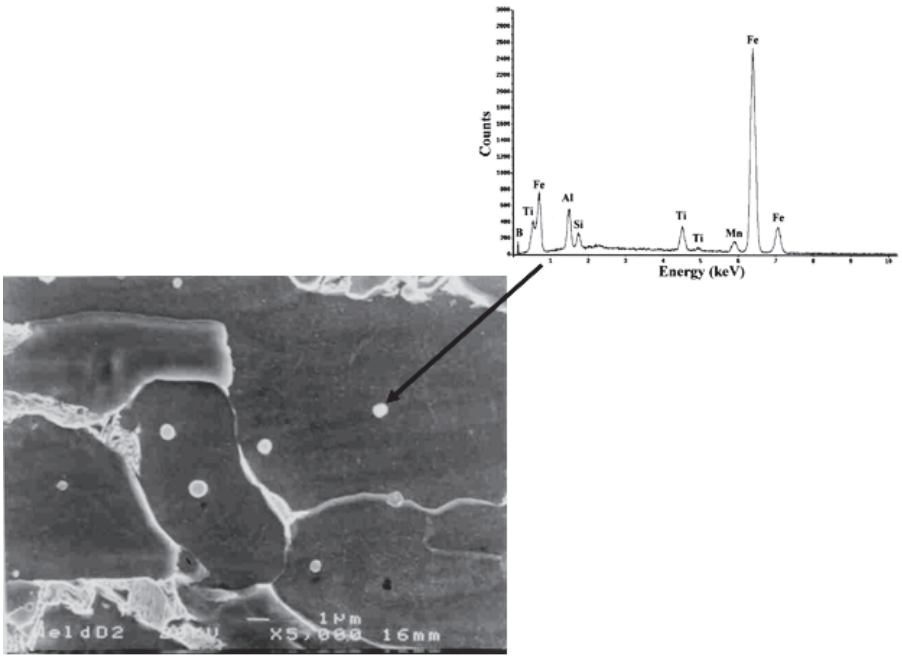

Fig. 10. SEM micrograph of Ti-Inclusions and it corresponding EDS spectrum.

3. Conclusion

The determination of phase in fluxes enables us to identify the different type of oxides and radicals formed during sintering of the initial materials. This quantification makes possible know what anions and cations will be present in the electric arc. The most reactive reacts quickly in the weld pool and might be either absorbed in the slag or retained in the weld as inclusions. In summary, this work shows the importance of the selection for flux composition in order to improve the mechanical properties of steel welds.

4. Acknowledgment

The authors wish to thank financial support from SIP-IPN-CONACYT.

5. References

Allen, A.W. (1966). Optical Microscopy in Ceramic Engineering, *Proceedings Of the Third Berkeley International Materials Conference* (6), p.p. 123-142. ISBN 471-28720-2 New York, United States.

Apold, A. (1962) *Carbon Oxidation in the Weld Pool*. Pergamon Press, the Macmillan Co., ISBN-10: 0080096921; ISBN-13: 978-0080096926, New York, United States.

ASM, 1989 *Metals Handbook*, vol. 8, Mechanical Testing 9th. Ed. pp. 39–74. ISBN: 087170389. Metals Park, OH, United States.

Babu, S.S. David, S.A. & Vitek, J.M. (1999) Thermo-chemical-mechanical effects on microstructure development in low-alloy steel welds elements, in: *Proceedings of the International Conference on Solid–Solid Phase Transformations'99 (JIMIC-3),* June, Kyoto, Japan.

Belton G.R; Moore, T. J. & Tankins E. S. (1963). Slag-metal reactions in submerged –arc welding. *Welding Journal Research. Suppl. Research*. 68 (3). pp. 289-290. ISSN: 00432296.

Belton G.R; Moore, T. J. & Tankins E. S. (1963). Slag-metal reactions in submerged –arc welding. *Welding Journal Research. Suppl. Research*. Vol. 68, No. 3, pp. 289-290. ISSN: 00432296.

Berry L. G. & Mason B. (1959) *Mineralogy*, Freeman (Ed.), pp. 150-155, ISBN: 13:978-0716702351, New York, USA.

Butler, C. A. & Jackson, C. E. (1967). Submerged-arc welding characteristics of the CaO-TiO2-SiO2, System, *Welding Journal Supplement Research*. Vol, 46 No, 10, pp. 448-456. ISSN: 00432296.

Christensen, N. & Gjermundsen, k.(1962) Measurements of Temperature Outside and in Weld Pool in Submerged Arc Welding. *U.S. Department of Army, Europea Research Office, Report No. 273091.*

Cullity, B. D., (2003) *Elements of X-ray Diffraction,* Addison Wesley(Ed.), 3a. Ed., p.p. 407-417. ISBN:13: 9780201011746, ISBN: 0201011743.

Davis, M.L.E. & Bailey N. (1991). Evidence from Inclusion Chemistry of Element Transfer during Submerged Arc Welding, *Journal Welding Research, Welding Research Supp*, Vol.70, No. 2, p.p. 58. ISSN: 00432296.

Davis, M.L. & Bailey, N. (1991) Evidence from inclusion chemistry of element transfer during submerged arc welding, *Welding Journal Supplement Research* Vol. 70 No. 2, 57– 61. ISSN: 00432296.

Davis, M.L.; & Bailey, N. (1991). Evidence from Inclusions Chemistry of Elements Transfer During Submerged Arc Welding. *Welding Journal, Supplement Research*, February, p.p. Vol.70, No. 2, pp. 61- 65, ISSN: 00432296.

Dowling, J.M. Corbett, H.W. & Kerr, (1986) Inclusion phases and the nucleation of acicular ferrite in submerged-arc welds in high-strength low alloy steels, *Metallurgical Transactions*. A Vol.17, No.9, 1613–1618. ISSN:0360-2133.

Dunham, W.B. & Christian, A. (1984). *Process Mineralogy of Ceramic Materials*, Elsevier Science (Ed), p.p. 20-48, ISBN: 0-444-00963-9, ISBN: 0-444-00963-9, New York, United States.

Evans, G.M. (1996) Microstructure and properties of ferritic steel welds containing Ti and B, *Welding Journal Supplement Research*.Vol. 75, No. 8, pp. 251– 254. . ISSN: 00432296.

Evans, G.M. (1996) Microstructure and Properties of Ferritic Steel Welds Cointaining Ti and B. *Welding Journal, Supplement Research*, August, p.p. 251-259. ISSN: 00432296.

Gordon, & Chu, P.K. (1966) Microstructure of Complex Ceramics. *Proceedings of the Third Berkeley International Materials Conference,* (6), p.p. 828-861. Berkeley Conference, CA, July . ISBN: 471-28720-2 USA New York United States.

Indacochea, J.E., Blander, M. & Shah, S. (1989). Submerged Arc Welding: Evidence for Electrochemical Effects on the Weld Pool, *Journal Welding Research Welding Supp.*, No. 3, p.p. 77-82, ISSN: 00432296.

Jackson, C.E., (1982). Submerged- Arc Welding Fluxes and Relations among Process Variables, *Metals Handbook, ASM, Metals*, p.p. 74-78. ISBN: 9780871706546, Park, Ohio, United States.

Joarder, A. Saha, S.C. & Ghose, A.K. (1991) Study of submerged arc weld metal and heat-affected zone microstructures of a plain carbon steel, *Welding Journal Supplement Research* Vol. 70 No. 6, pp. 141–146. ISSN: 00432296.

Klein, C. & Hurbult, C. S. (1999) *Manual of Mineralogy*, Wiley, (Ed.), 566-567. ISBN-10: 0471821829, ISBN-13: 978-0471821823, New York, United States.

Lancaster, J.F. (1999) *Metallurgy of Welding*, Alden Press Ltd., London, 1980, pp. 25-50, Woodhead publication, 6a. (Ed.) p.p. 110-177. ISBN: 0046690042 / 0-04-669004-2, Hertfordshire, HRT, United Kingdom.

Liu, S. & Olson, D.L. (1986) The role of inclusions in controlling HSLA steel weld microstructures, *Welding Journal Supplement Research* Vol.65, No. 6, pp. 139–141, ISSN: 00432296.

Liu, S. & Olson, D.L. (1986). The role of inclusions in controlling HSLA steel weld microstructures, *Welding Journal Supplement Research* Vol. 65, No.6, pp. 144– 149, ISSN: 00432296.

Material Algorithms Project, (1999) MAP: Perpetual Library of Computer Programs, Available from www.msm.cam.ac.uk/map/mapmain.html.

Redwine R. H. & Conrad M. A., (1966), Microstructures developed in crystallized glass-ceramics in: *Proceedings in the Third Berkeley International Materials Conference*, No. 40, pp. 900- 922, Berkeley Conference, CA, July . ISBN: 471-28720-2 USA New York.

Shah, S. (1986). *The Influence of Flux Composition on the Microstructure and Mechanical Properties of Low-carbon Steel Weld Metal*, M.S. Thesis, University of Illinois, Chicago Ill. United States.

Singer, F.; & Singer, S. (1979) Cerámica Industrial , Enciclopedia de la Química Industrial Tomo 9, Vol. 1, ed. URMO, S.A (Ed.), 236-257, ISBN 84-314 -0177-X, Bilbao, España.

Vander Eijk, Grong, C. O. Hjelen, J. (1999) Quantification of inclusions stimulated ferrite nucleation in wrought steel using the SEM EBSD technique, in: *Proceedings of the International Conference on Solid–Solid Phase Transformations'99 (JIMIC-3), pp.* 351, *Kyoto, Japan*, June.

Zhang, M. He, K. & Edmons, D.V. (1999) Formation of acicular ferrite in C–Mn steels promoted by vanadium alloying elements, in: *Proceedings of the International Conference on Solid–Solid Phase Transformations' 99 (JIMIC-3), Kyoto, Japan*, June.

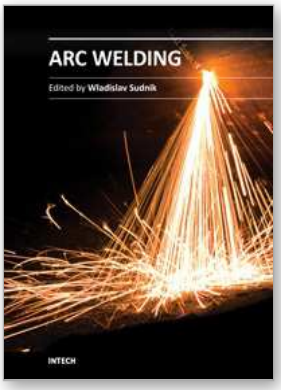

Arc Welding

Edited by Prof. Wladislav Sudnik

ISBN 978-953-307-642-3
Hard cover, 320 pages
Publisher InTech
Published online 16, December, 2011
Published in print edition December, 2011

Ever since the invention of arc technology in 1870s and its early use for welding lead during the manufacture of lead-acid batteries, advances in arc welding throughout the twentieth and twenty-first centuries have seen this form of processing applied to a range of industries and progress to become one of the most effective techniques in metals and alloys joining. The objective of this book is to introduce relatively established methodologies and techniques which have been studied, developed and applied in industries or researches. State-of-the-art development aimed at improving technologies will be presented covering topics such as weldability, technology, automation, modelling, and measurement. This book also seeks to provide effective solutions to various applications for engineers and researchers who are interested in arc material processing. This book is divided into 4 independent sections corresponding to recent advances in this field.

InTech Europe
University Campus STeP Ri
Slavka Krautzeka 83/A
51000 Rijeka, Croatia
Phone: +385 (51) 770 447
Fax: +385 (51) 686 166
www.intechopen.com

InTech China
Unit 405, Office Block, Hotel Equatorial Shanghai
No.65, Yan An Road (West), Shanghai, 200040, China
中国上海市延安西路65号上海国际贵都大饭店办公楼405单元
Phone: +86-21-62489820
Fax: +86-21-62489821